

# Inference-Time Scaling for Visual AutoRegressive modeling by Searching Representative Samples

Weidong Tang, Xinyan Wan, Siyu Li, and Xiumei Wang<sup>(✉)</sup>

School of Electronic Engineering, Xidian University, Xi'an, China  
 wangxm@xidian.edu.cn

**Abstract.** While inference-time scaling has significantly enhanced generative quality in large language and diffusion models, its application to vector-quantized (VQ) visual autoregressive modeling (VAR) remains unexplored. We introduce **VAR-Scaling**, the first general framework for inference-time scaling in VAR, addressing the critical challenge of discrete latent spaces that prohibit continuous path search. We find that VAR scales exhibit two distinct pattern types: general patterns and specific patterns, where later-stage specific patterns conditionally optimize early-stage general patterns. To overcome the discrete latent space barrier in VQ models, we map sampling spaces to quasi-continuous feature spaces via kernel density estimation (KDE), where high-density samples approximate stable, high-quality solutions. This transformation enables effective navigation of sampling distributions. We propose a density-adaptive hybrid sampling strategy: Top- $k$  sampling focuses on high-density regions to preserve quality near distribution modes, while Random- $k$  sampling explores low-density areas to maintain diversity and prevent premature convergence. Consequently, VAR-Scaling optimizes sample fidelity at critical scales to enhance output quality. Experiments in class-conditional and text-to-image evaluations demonstrate significant improvements in inference process. The code is available at <https://github.com/WD7ang/VAR-Scaling>.

**Keywords:** Inference-time scaling · Visual AutoRegressive modeling (VAR) · Vector quantization (VQ)

## 1 Introduction

Recent research has yielded significant advances in inference-time scaling laws for generative models [22, 17, 36]. Large language models (LLMs) demonstrate powerful implicit chain-of-thought (CoT) capabilities by emulating deliberate, System 2-like reasoning [14, 7, 35, 39], internally exploring multi-step, multi-path solutions to select optimal outputs. Concurrently, a new scaling paradigm has emerged in diffusion models [21]: instead of increasing denoising steps, researchers now use verifiers with intelligent search algorithms to actively explore noise space for superior paths [19]. This approach strategically leverages extra computation via directed search, significantly boosting the quality of output.

While inference-time scaling uses LLMs and diffusion models, it remains unexplored in VQ generative models. Currently, the state-of-the-art VQ framework, VAR achieves superior fidelity through its “next-scale prediction” paradigm [31]. Therefore we adopt VAR [31] as the baseline to evaluate novel scaling strategies

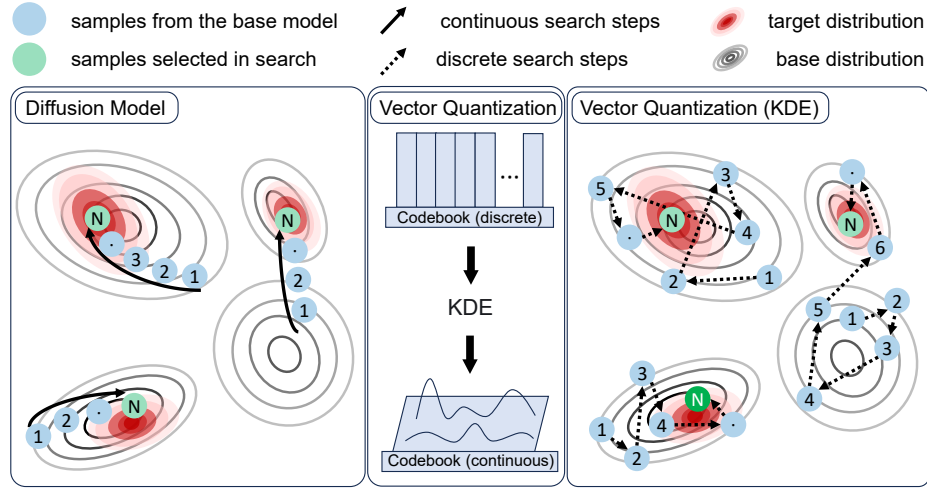


Fig. 1: Diffusion models enable metric-guided continuous search from base to target distributions. In contrast, VQ’s discrete nature prevents continuous path exploration. Our KDE mapping transforms probability-scaled sampling spaces into continuous trajectories, eliminating chaotic unguided searches evident.

for discrete generative spaces. Crucially, as VAR operates through a coarse-to-fine generation process, the quality of final output is primarily determined by the quality of coarse scale sampling decisions [31]. In the VAR inference process, We find that: *i*) General patterns, *e.g.*, categories, object outlines, are identified in the beginning inference iterations; *ii*) Specific patterns, *e.g.*, texture details, edge refinements, are incrementally incorporated in the later inference iterations<sup>1</sup>. Consequently, improving coarse-scale sampling quality directly minimizes initial error sources, thereby mitigating downstream propagation effects.

Therefore, to enhance sampling quality at specific coarse scales, we must address two fundamental challenges: *i*) defining what constitutes representative samples, and *ii*) developing efficient methods to identify them. As shown in Figure 1, while diffusion models locate high quality samples through noise space search guided by verifier scores [24, 30], the discrete latent space of VQ models impedes direct transfer of such approaches. Consequently, we conduct dedicated analysis for discrete spaces by implementing two baseline strategies: random-k, top-k and small-k sampling to evaluate how sampling strategies impact VAR’s performance across different sample sizes. Through empirical observations of VAR’s inference process, we find that repeated sampling from the predictive distribution enables KDE-based Euclidean mapping. This transforms discrete sampling spaces into quasi-continuous feature spaces. Within these spaces, high-density samples represent the most characteristic outputs<sup>2</sup>.

<sup>1</sup> Detailed implementations about these vanilla methods are in Sec. 3.2

<sup>2</sup> Detailed implementations about these vanilla methods are in Sec. 3.3

Therefore, we propose **VAR-Scaling**, the first framework for inference time scaling in VAR. Our approach progressively clarifies representative samples at specific coarse scales of VAR by expanding the sample space, while strategically preserving diversity through density-adaptive sampling: when high-density regions are detected in the current distribution, we employ top-k sampling; otherwise, random-k sampling is activated. This architecture unlocks VAR’s latent potential without exhaustive discrete space search, achieving significant performance gains through intelligent sampling allocation.

Our method demonstrates effective performance in both class-conditional and text-conditional image generation. We conduct comparative testing against VAR and its relevant works. The contributions are as follows:

1. We propose VAR-Scaling, the first general framework for inference-time scaling in VAR. We show that searching representative samples through scaling number of samples can lead to improvement generation tasks.
2. Based on experiments, we approximately map the discrete space to the continuous space, and empirically define the sample with the highest density as the representative sample. It provides a new idea for the inference time scaling of discrete Spaces for the first time.
3. The evaluation results on VAR, FlexVAR [13], and Infinity [10] demonstrate that VAR and FlexVAR improve the IS [25] score by 8.7% and 6.3% respectively while maintaining stable FID [11]. On Infinity, the Geneval score increases 1.1%.

## 2 Related Work

### 2.1 Inference-time scaling

In recent years, inference-time scaling for LLMs has seen remarkable progress [1, 8, 36, 27]. Approaches that integrate search algorithms with LLMs have emerged, such as breadth - first search [33], depth - first search [29], Monte Carlo Tree Search [2], and guided beam search [23, 37]. These methods highlight the benefits of incorporating search during inference, as they can boost performance across various tasks. In addition, process reward models (PRM) [38] have proven effective in selecting reasoning paths with low error rates and providing rewards within reinforcement learning - style algorithms [16, 20, 34]. By rewarding intermediate steps, PRM can guide multi - step reasoning processes [18]. However, the application of these approaches in the field of image generation has been limited. While some recent research has focused on iterative processes in diffusion models [12, 28, 4] and the use of Chain of Thought (CoT) for self - correction in autoregressive image generation [15, 5], visual autoregressive models based on VQ models have not been thoroughly investigated.

### 2.2 Autoregressive Visual Generation

The visual autoregressive models based on VQ use vector quantization to convert image patches into index tokens. These tokens are predicted at a coarse scale and then used to predict and fuse the residual image patches at the next scale, gradually generating a finer-resolution image [31, 15]. However, due to the limitations

of quantization errors, this approach struggles to further improve performance, especially in generating high-resolution images where details are often compromised [6, 32]. To address this issue, the VAR-based Infinity model employs an almost infinitely large continuous tokenizer, bypassing the limitations of discrete quantization and significantly enhancing generation quality [38]. By using continuous tokens, the model is able to handle image generation more precisely, improving the depiction of finer details.

### 3 Methodology

In this Section, we first introduce VAR [31] and KDE in Section 3.1. Sec. 3.2 establishes coarse-scale sampling quality as the fidelity determinant in VAR. Three inference search strategies reveal sample distribution properties, yielding our density-guided algorithm from empirical data.

#### 3.1 Preliminary

**Generative Priors in VAR.** Different from traditional autoregressive methods, VAR redefines image generation as a coarse-to-fine task. In VAR, the autoregressive unit is an entire token map, rather than a single token. It starts by quantizing a feature map  $f \in \mathbb{R}^{h \times w \times C}$  into  $K$  multi-scale token maps  $(r_1, r_2, \dots, r_K)$ , each at a increasingly higher resolution  $h_k \times w_k$ , culminating in  $r_K$  matches the original feature map's resolution  $h \times w$ . The autoregressive likelihood is formulated as:

$$p(r_1, r_2, \dots, r_K) = \prod_{k=1}^K p(r_k | r_1, r_2, \dots, r_{k-1}), \quad (1)$$

where each autoregressive unit  $r_k \in [V]^{h_k \times w_k}$  is the token map at scale  $k$  containing  $h_k \times w_k$  tokens, and the sequence  $(r_1, r_2, \dots, r_{k-1})$  serves as the the “prefix” for  $r_k$ .

**Density estimation.** KDE is a non-parametric method for estimating unknown probability density functions from finite samples. Given  $n$  candidate tokens  $\{x_i\}_{i=1}^n \subset \mathbb{R}^d$  sampled from a discrete codebook, the multivariate density estimator with isotropic Gaussian kernel [26] is defined as:

$$\hat{f}(x) = \frac{1}{n(2\pi)^{d/2}h^d} \sum_{i=1}^n \exp\left(-\frac{\|x - x_i\|^2}{2h^2}\right) \quad (2)$$

where  $h > 0$  is the bandwidth parameter controlling smoothness, and  $d$  denotes the embedding dimension. The bandwidth selection follows Silverman's rule generalized for multivariate data:

$$h = \sigma \left[ \frac{n(d+2)}{4} \right]^{-1/(d+4)} \quad (3)$$

where  $\sigma$  is the dimension-wise mean standard deviation  $\frac{1}{d} \sum \sigma_j$ . The exponential term  $\exp(-\|x - x_i\|^2/(2h^2))$  measures similarity between tokens, with the summation reflecting density accumulation from neighboring samples.

### 3.2 The inference process of VAR.

VAR employs a progressive refinement strategy across multi-scale stages  $k \in \{0, 1, 2, \dots, 9\}$ . At scale  $k$ , the model decodes a multi-scale token map  $r_k$  (resolution  $h_k \times w_k$ ) to generate output images:

$$I_k = D(r_k), \quad (4)$$

where  $I_k$  denotes the generated image at scale  $k$ , and  $D$  represents the decoder function. The process initiates from a low resolution base ( $k = 1$ ) and incrementally adds details. To investigate the boundary between universal and specific patterns, we substituted the random number generator at scale  $k$  and observed resultant variations in the final decoding output.

#### Analysis of Perturbation

**Results.** Figure 2 shows that perturbing at scale 1 leads to significant divergence, highlighting its critical role in defining the final image's spatial structure. At scale 2, differences are noticeably smaller. Subsequent scales refine initial selections with perceptually nuanced variants, incorporating fine details into established general patterns, enhancing overall image quality.

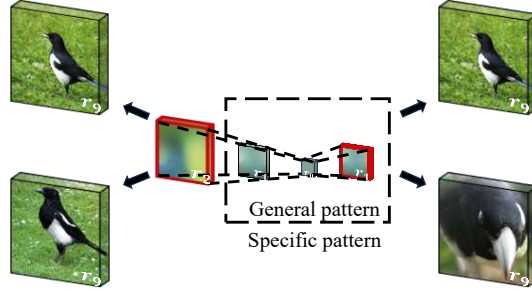


Fig. 2: Scales 0-1 define general patterns like spatial structures and contours; scales 2-9 refine specific patterns with texture, edge, and local feature enhancements.

### 3.3 Inference-time Scaling on VAR.

To identify representative samples, we first assess inter-sample distances via Euclidean metric, then compute density scores using KDE. Three baseline selection strategies are proposed:

**Top- $k$  Sampling.** Density-guided sampling selects representative samples that balance diversity and quality, selecting the top  $k$  highest-density samples and using their densities as selection probabilities.

$$S_{\text{top-}k} = \{x_i \mid x_i \in \arg \max_{x \in \mathcal{X}} \hat{f}(x), i = 1, 2, \dots, k\}, \quad (5)$$

$$\text{Top}_k(m, \mathcal{X}) := \begin{cases} \arg \max_{|\kappa|=k, \kappa \subset \mathcal{X}} \sum_{\kappa_j \in \kappa} m(\kappa_j), & \text{if } |\mathcal{X}| > k, \\ \mathcal{X}, & \text{otherwise.} \end{cases} \quad (6)$$

where  $\mathcal{X}$  is the sampling space and  $\hat{f}(x)$  is the density score of sample  $x$ . The probability of selecting each sample  $x_i$  is normalized.

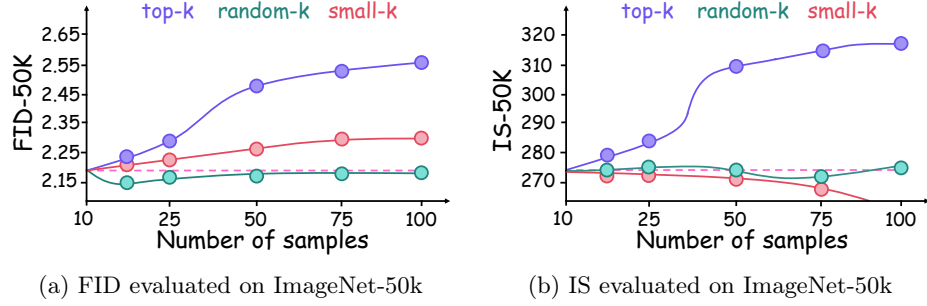


Fig. 3: For ImageNet generation, we report model performance using the standard evaluation metrics, FID  $\downarrow$  [11] and IS  $\uparrow$  [25]. Our experiments show that high-density samples are likely representative prototypes, while low-density samples may correspond to low quality outliers.

However, as shown in Figure 3, with inference time scaling, although IS increases significantly, FID rises uncontrollably. This is because as the sampling space expands, the distribution characteristics of samples become more apparent. This biased search leads to multiple samplings of certain representative samples, causing low variance and high similarity among samples. This guided search approach shares conceptual similarities with *reward hacking* in reinforcement learning, and existing research terms this phenomenon as *verifier hacking* [19].

**Small- $k$  Sampling.** As a conceptual counterpart to Top- $k$  sampling, Small- $k$  sampling selects the  $k$  samples with the lowest density scores.

As shown in Figure 3, to validate the Top- $k$  strategy inversely, we observe that sampling low-density regions leads to a decrease in IS while simultaneously causing FID to rise due to the density guided search mechanism.

**Random- $k$  Sampling.** We randomly select  $k$  samples from the sampling space  $\mathcal{X}$ . Then, based on the density scores of these  $k$  samples, we choose one final sample:

$$S_{\text{random-}k} = \{x_i \mid x_i \in \mathcal{X}, i = 1, 2, \dots, k\}, \quad (7)$$

$$\text{Random}_k(m, \mathcal{X}) := \begin{cases} \text{sample } \mathcal{P}(\kappa), \text{if } |\mathcal{X}| > k, \\ \mathcal{X}, \text{otherwise,} \end{cases} \quad (8)$$

where  $\mathcal{P}(\kappa)$  is the probability distribution over subsets  $\kappa \subset \mathcal{X}$ . The probability of selecting each sample  $x_i$  is normalized.

However, as shown in Figure 3, with inference time scaling, although FID remains stable, the improvement in IS is limited. This is due to the lack of a guiding mechanism for finding representative samples.

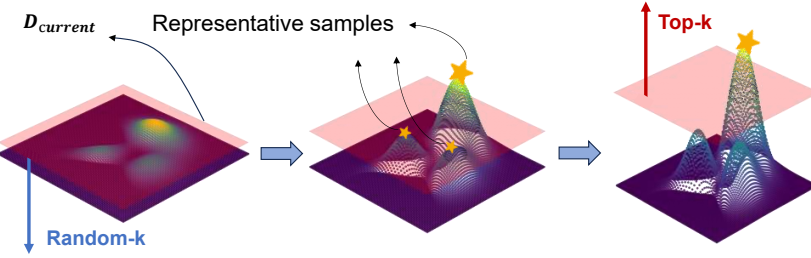


Fig. 4: Across successive expansion iterations (left → right), the representative samples of distribution exhibits progressive structural refinement.

**Density-guided representative samples (VAR-Scaling).** To balance the diversity of categories and the quality of images, our examination of Section 3.3 shows that the characteristics of the subspace fall into two categories: *i*). High-density regions: Samples in these regions may correspond to archetypal, stable patterns intensively learned from training data, characterized by highly concentrated distribution. *ii*). Low-density regions: Samples in these regions may represent marginal cases or outliers within the model’s predictive distribution, characterized by highly scattered distribution.

Based on these findings, we adopt different sampling strategies: *i*). For high-density regions, we apply top-k sampling. *ii*). For low-density regions, we use random-k sampling. As shown in Figure 4, the details on how to distinguish between high and low density are as follows:

$$\begin{cases} \text{Density Mean} = \frac{1}{n} \sum_{i=1}^n \hat{f}(x_i) \\ D_{\text{current}} = \text{Density Mean} \times \alpha \end{cases} \quad (9)$$

where  $n$  is the number of samples, and  $\hat{f}(x_i)$  is the density score of sample  $x_i$ .  $\alpha$  is the density threshold coefficient. Finally, we can get:

$$\text{Density Classification} = \begin{cases} \text{low-density} & \text{if } D_{\text{current}} < D_{\text{max}} \\ \text{high-density} & \text{otherwise} \end{cases}$$

## 4 Experiments

### 4.1 Settings

**Datasets and models.** For VAR [31] and FlexVAR [13], we conduct experiments on the ImageNet [3] 256×256 conditional generation benchmark such as Fréchet inception distance (FID [11]), inception score (IS [25]). For evaluation of Infinity models, we report results on text-to-image benchmarks like GenEval [9].

**Implementation details.** The comprehensive standard experimental configurations for all models are meticulously listed in Table 1. This table explicitly specifies the default settings consistently used throughout the experiments.

Table 1: Default configuration and recommended parameter range.

(a) The default configurations of the three models.

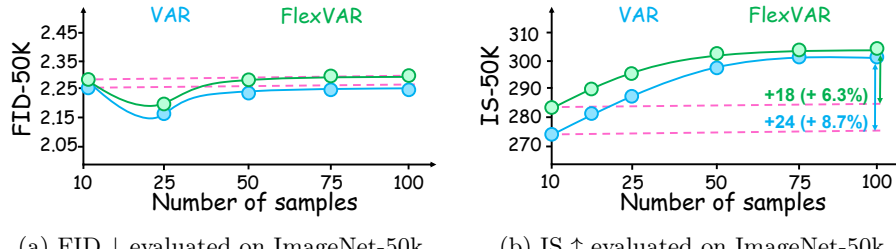
default	VAR [31]	FlexVAR [13]	Infinity [10]
GPU	A6000 48GB	A6000 48GB	A100 40GB
scale	1	2	3
model size	16/20/24/30	24	2B
number of samples (#n)	10-100	10-100	500-3000
Classifier-Free Guidance (cfg)	1.0	2.5	4.0
representative samples (#rep)	10	10	500

(b) density threshold coefficient range recommended.

default	VAR [31]	Flex-VAR [13]	Infinity [10]
size	d16	d20	d24
$\alpha$	2.3 - 2.9	2.2 - 2.8	2.1 - 2.7

## 4.2 Image Generation

**Evaluations on class-conditional and text-conditional image generation benchmarks.** As shown in Figures 5 and 6, VAR-Scaling achieves notable inference gains in both class-conditional (VAR [31], FlexVAR [13]) and text-to-image (Infinity [10]) tasks: +8.7% IS [25], +6.3% IS, and +1.1% Geneval [9].



(a) FID ↓ evaluated on ImageNet-50k

(b) IS ↑ evaluated on ImageNet-50k

Fig. 5: Experimental results demonstrate that high-density regions correspond to representative samples, whereas low-density samples are low-quality samples.

**Analyses.** Given that VAR and FlexVAR employ VQ while Infinity utilizes binary spherical quantization (BSQ [40]), we accordingly configure distinct search times to construct appropriately-sized sampling spaces for identifying optimal representative samples.

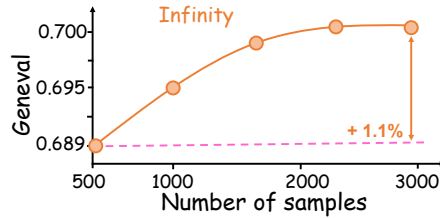


Fig. 6: Geneval ↑ Evaluation of Infinity

### 4.3 Ablation Study

In this section, we carry out a series of ablation studies to explore various interesting features of VAR-Scaling in different scenarios. Unless noted, all experiments follow the default configuration and report mean performance.

VAR						
scale	[H,W]	number of samples	representative samples	$\alpha$	FID $\downarrow$	IS $\uparrow$
-	-	-	-	-	2.25	274.7
0	[1,1]	20	10	2.3	2.44	285.2
	[1,1]	50	10	2.4	3.07	288.2
	[1,1]	100	10	2.5	2.91	296.0
1	[2,2]	20	10	2.3	2.16	279.3
	[2,2]	50	10	2.4	2.25	298.7
	[2,2]	100	10	2.4	2.19	295.2
2	[3,3]	20	10	1.7	2.18	283.3
	[3,3]	50	10	1.7	2.25	298.3
	[3,3]	100	10	1.8	2.24	296.2
3	[4,4]	20	10	1.9	2.17	283.2
	[4,4]	50	10	1.9	2.23	289.4
	[4,4]	100	10	1.8	2.33	291.1
4	[5,5]	20	10	1.9	2.19	288.2
	[5,5]	50	10	1.9	2.21	295.8
	[5,5]	100	10	2.0	2.12	288.3
5	[6,6]	20	10	1.8	2.21	289.0
	[6,6]	50	10	1.8	2.25	293.0
	[6,6]	100	10	2.0	2.10	285.4
6	[8,8]	20	10	1.7	2.10	284.3
	[8,8]	50	10	1.7	2.26	288.2
	[8,8]	100	10	1.9	2.09	285.4
7	[10,10]	20	10	1.4	2.18	286.5
	[10,10]	50	10	1.4	2.20	287.1
	[10,10]	100	10	1.5	2.11	284.7
8	[13,13]	20	10	1.2	2.18	282.7
	[13,13]	50	10	1.2	2.24	286.2
	[13,13]	100	10	1.3	2.12	284.5
9	[16,16]	20	10	1.1	2.19	280.2
	[16,16]	50	10	1.1	2.23	284.3
	[16,16]	100	10	1.3	2.16	281.8

Table 2: Ablation on scales  $\in \{0, 1, 2, 3, 4, 5, 6, 7, 8, 9\}$  and all scales  $\geq 1$ . Scaled 1 is selected, considering the cost of high scales and performance.

**Ablation on scales.** Aimed at identifying the most critical scale for sampling, we conducted multi-scale experiments on general patterns. Setting: We change the default scale. Detailldly, we select the d30 model of VAR, use L2 distance as the distance metric, set the cfg weight to 1.0, and follow the sampling number, coresets size, and  $\alpha$  settings shown in Table. 1. We conduct experiments at each scale and compare the FID [11] and IS [25] results. Based on Table. 2 it

Table 3: Ablation experiment result chart.

(a) Ablation study on model sizes. VAR [31] d30 is selected, considering it better demonstrates the effectiveness of the method.

model	number of samples	representative samples	$\alpha$	FID $\downarrow$	IS $\uparrow$
VAR-d16	-	-	-	3.81	227.2
	20	10	2.4	3.77	227.5
	50	10	2.4	3.75	228.3
	100	10	2.6	3.69	232.6
VAR-d20	-	-	-	2.84	253.3
	20	10	2.3	2.72	267.4
	50	10	2.4	2.81	262.3
	100	10	2.5	2.78	261.0
VAR-d24	-	-	-	2.28	273.7
	20	10	2.7	2.18	275.2
	50	10	2.7	2.24	276.3
	100	10	2.8	2.21	280.3
VAR-d30	-	-	-	2.25	274.7
	20	10	2.3	2.16	279.3
	50	10	2.4	2.25	298.7
	100	10	2.4	2.19	295.2

(b) Ablation study on different strategies. Selected VAR-Scaling, considering performance.

strategy	#n	#rep	$\alpha$	FID $\downarrow$	IS $\uparrow$
-	-	-	-	2.25	274.7
VAR-Scaling	20	10	2.3	2.16	279.3
	50	10	2.4	2.25	298.7
	100	10	2.4	2.19	295.2
top-k	20	10	-	2.30	296.9
	50	10	-	2.46	304.7
	100	10	-	2.42	301.5
random-k	20	10	-	2.25	276.1
	50	10	-	2.27	276.7
	100	10	-	2.24	275.3

(d) Ablation study on  $\text{cfg} \in \{1.0, 1.5, 2.0\}$ .  $\text{cfg}=1.0$  is selected to minimize the influence of  $\text{cfg}$  and demonstrate the capability of VAR-Scaling in the base model, focusing on the simple conditional generation task without guidance.

cfg	#n	#rep	$\alpha$	FID $\downarrow$	IS $\uparrow$
-	-	-	-	2.25	274.7
$\text{cfg}=1.0$	20	10	2.3	2.16	279.3
	50	10	2.4	2.25	298.7
	100	10	2.4	2.19	295.2
$\text{cfg}=1.5$	-	-	-	2.01	305.7
	20	10	1.8	1.97	310.4
	50	10	1.8	2.16	320.4
	100	10	1.9	2.13	319.1

(c) Ablation study on coresnet size. A size of 10 is selected, balancing model performance and computational cost.

#n	#rep	$\alpha$	FID $\downarrow$	IS $\uparrow$
-	-	-	2.25	274.7
5	20	2.3	2.17	279.0
	50	2.4	2.23	297.5
	100	2.4	2.21	295.1
10	20	2.3	2.16	279.3
	50	2.4	2.25	298.7
	100	2.4	2.19	295.2
15	20	2.3	2.13	278.8
	50	2.4	2.24	298.4
	100	2.4	2.17	294.0

(e) Ablation study on distance metrics. ED: Euclidean Distance, CS: Cosine Similarity. Euclidean Distance is selected as it more effectively captures scaling patterns during inference, particularly showcasing consistent performance gains across varying model configurations.

metric	#n	#rep	$\alpha$	FID $\downarrow$	IS $\uparrow$
-	-	-	-	2.25	274.7
ED	20	10	2.3	2.16	279.3
	50	10	2.4	2.25	298.7
	100	10	2.4	2.19	295.2
CS	20	10	2.3	2.23	296.8
	50	10	2.4	2.21	293.0
	100	10	2.4	2.18	288.1

is clear that each scale has a different weight. When  $\text{scale} = 0$ , tuning the hyperparameters also struggles to control FID, as VAR-Scaling introduces biased information too early, causing the search to converge prematurely to the verifier's bias. For  $\text{scale} \in \{2, 3, 4\}$ , their effects are very similar, but they require more computational resources compared to  $\text{scale} = 1$ . Scales  $\in \{5, 6, 7, 8, 9\}$  are specific patterns that mainly affect local details, resulting in a smaller improvement. Overall, through numerous experiments, we explained that the importance and effects of the VAR [31] scales vary, and we selected  $\text{scale} = 1$  as the optimal processing layer.

**Ablation on model sizes.** To investigate the generalization of VAR-Scaling under different model sizes, we conducted experiments. Setting: We change the default model size and density threshold coefficient. As shown in Table. 3a, experiments demonstrate that our method generalizes across different model sizes, and we have found that the optimal configuration is constantly changing, with no universal solution.

**Ablation on different strategies.** VAR-Scaling's efficacy is validated through comparisons with top-k and random-k methods. Table 3b shows top-k improves IS [25] over random-k but misaligns with FID [11] objectives by prioritizing single-sample quality over population diversity. This diversity deficit reduces sample variance, inducing mode collapse at larger sampling sizes. Random-k's unconstrained search yields marginal gains. VAR-Scaling successfully integrates both approaches' strengths, confirming our design rationale.

**Ablation on the number of representative samples.** To explore the impact of different number of representative samples on VAR-Scaling, we conducted experiments. Setting: we vary the number of representative samples. As shown in Table. 3c, experiments demonstrate that our method is insensitive to the size of the core set. This means that the samples selected by VAR-scaling are representative, and we have proven that the representative samples are indeed the central samples.

**Ablation on classifier-free guidance.** To investigate the generalization of VAR-Scaling under different classifier-free guidance weights, we conducted experiments. Setting: We change the default classifier-free guidance  $\in \{1.0, 1.5, 2.0\}$ . As shown in Table. 3d, the study found that our method is effective not only when guidance is not used, but also under strong classifier-free guidance weight influence, where our method can further enhance the performance. This indicates that our method generalizes across different classifier-free guidance.

**Ablation on distance metric.** Comparisons of Euclidean distance and cosine similarity reveal key robustness properties. As shown in Figure 3e, the marginal differences in FID/IS metrics further demonstrate VAR-Scaling's strong flexibility across diverse measurement choices.

#### 4.4 Visualization

In this section, we present abundant visualization of VAR-Scaling’s outputs on Infinity [10]. Figure 7 demonstrates that in inference-time scaling process, the generated outputs exhibit increasing alignment with prompt specifications, particularly for quantitative evaluation tasks such as counting.



“Two boy, a dog and two cats are running in the field.”



“Four planes are flying in the air.”

Fig. 7: The visualization of VAR-Scaling’s segmentation results on Infinity. As the scaling increases, the quality of the image becomes more stable and is better able to focus on the information provided by the prompt.

## 5 Conclusion and Future Work

In this work, we propose the first framework for inference time scaling in VAR. It provides a new approach for the inference time scaling of discrete spaces for the first time. Extensive experiments have supported our method’s effectiveness, and a series of ablation studies also validates its robustness in data and parameters. However, our method does have some limitations: *i*). The theoretical linkage between high-density samples and high-quality representative samples warrants deeper investigation. *ii*). VAR-Scaling has not yet been applied to video generation models. Conclusively, our method is an effective solution for VAR, and we hope to inspire future researches in generative model optimization.

**Acknowledgments.** This research was funded in part by the National Natural Science Foundation of China under Grant 62372355, in part by the Natural Science Basic Research Program of Shaanxi Province under Grant 2023-JC-ZD-39 and 2024JC-YBMS-520, in part by the Open Fund of State Key Laboratory of Intelligent Manufacturing of Advanced Construction Machinery(KFKT2024008).

## References

- [1] Alexander Borzunov, Max Ryabinin, Artem Chumachenko, Dmitry Baranchuk, Tim Dettmers, Younes Belkada, Pavel Samygin, and Colin A. Raffel. Distributed Inference and Fine-tuning of Large Language Models Over The Internet. In *NeurIPS*, 2023.
- [2] Cameron Browne, Edward Jack Powley, Daniel Whitehouse, Simon M. Lucas, Peter I. Cowling, Philipp Rohlfshagen, Stephen Tavener, Diego Perez Liebana, Spyridon Samothrakis, and Simon Colton. A Survey of Monte Carlo Tree Search Methods. *IEEE Trans. Comput. Intell. AI Games*, 4: 1–43, 2012.
- [3] Jia Deng, Wei Dong, Richard Socher, Li-Jia Li, Kai Li, and Li Fei-Fei. ImageNet: A large-scale hierarchical image database. In *CVPR*, pages 248–255, 2009.
- [4] Prafulla Dhariwal and Alexander Quinn Nichol. Diffusion Models Beat GANs on Image Synthesis. In *NeurIPS*, pages 8780–8794, 2021.
- [5] Patrick Esser, Robin Rombach, Andreas Blattmann, and Björn Ommer. Imagebart: Bidirectional Context with Multinomial Diffusion for Autoregressive Image Synthesis. In *NeurIPS*, pages 3518–3532, 2021.
- [6] Patrick Esser, Robin Rombach, and Björn Ommer. Taming Transformers for High-Resolution Image Synthesis. In *CVPR*, pages 12873–12883, 2021.
- [7] Hao Fei, Bobo Li, Qian Liu, Lidong Bing, Fei Li, and Tat-Seng Chua. Reasoning Implicit Sentiment with Chain-of-Thought Prompting. In *ACL*, pages 1171–1182, 2023.
- [8] Jonas Geiping, Sean McLeish, Neel Jain, John Kirchenbauer, Siddharth Singh, Brian R. Bartoldson, Bhavya Kailkhura, Abhinav Bhatele, and Tom Goldstein. Scaling Up Test-Time Compute with Latent Reasoning: A Recurrent Depth Approach. *arXiv preprint arXiv:2502.05171*, 2025.
- [9] Dhruba Ghosh, Hannaneh Hajishirzi, and Ludwig Schmidt. GenEval: An Object-Focused Framework for Evaluating Text-to-Image Alignment. In *NeurIPS*, 2023.
- [10] Jian Han, Jinlai Liu, Yi Jiang, Bin Yan, Yuqi Zhang, Zehuan Yuan, Bingyue Peng, and Xiaobing Liu. Infinity: Scaling Bitwise Autoregressive Modeling for High-Resolution Image Synthesis. In *CVPR*, pages 15733–15744, 2025.
- [11] Martin Heusel, Hubert Ramsauer, Thomas Unterthiner, Bernhard Nessler, and Sepp Hochreiter. GANs Trained by a Two Time-Scale Update Rule Converge to a Local Nash Equilibrium. In *NeurIPS*, pages 6626–6637, 2017.
- [12] Jonathan Ho, Ajay Jain, and Pieter Abbeel. Denoising Diffusion Probabilistic Models. In *NeurIPS*, 2020.
- [13] Siyu Jiao, Gengwei Zhang, Yinlong Qian, Jiancheng Huang, Yao Zhao, Humphrey Shi, Lin Ma, Yunchao Wei, and Zequn Jie. Flexvar: Flexible Visual Autoregressive Modeling without Residual Prediction. *arXiv preprint arXiv:2502.20313*, 2025.
- [14] Takeshi Kojima, Shixiang Shane Gu, Machel Reid, Yutaka Matsuo, and Yusuke Iwasawa. Large Language Models are Zero-Shot Reasoners. In *NeurIPS*, 2022.

- [15] Doyup Lee, Chiheon Kim, Saehoon Kim, Minsu Cho, and Wook-Shin Han. Autoregressive Image Generation using Residual Quantization. In *CVPR*, pages 11513–11522, 2022.
- [16] Harrison Lee, Samrat Phatale, Hassan Mansoor, Thomas Mesnard, Johan Ferret, Kellie Lu, Colton Bishop, Ethan Hall, Victor Carbune, Abhinav Rastogi, and Sushant Prakash. RLAIF vs. RLHF: Scaling Reinforcement Learning from Human Feedback with AI Feedback. In *ICML*, 2024.
- [17] Yaniv Leviathan, Matan Kalman, and Yossi Matias. Fast Inference from Transformers via Speculative Decoding. In *ICML*, pages 19274–19286, 2023.
- [18] Hunter Lightman, Vineet Kosaraju, Yuri Burda, Harrison Edwards, Bowen Baker, Teddy Lee, Jan Leike, John Schulman, Ilya Sutskever, and Karl Cobbe. Let’s Verify Step by Step. In *ICLR*, 2024.
- [19] Nanye Ma, Shangyuan Tong, Haolin Jia, Hexiang Hu, Yu-Chuan Su, Mingda Zhang, Xuan Yang, Yandong Li, Tommi S. Jaakkola, Xuhui Jia, and Saining Xie. Inference-Time Scaling for Diffusion Models beyond Scaling Denoising Steps. *arXiv preprint arXiv:2501.09732*, 2025.
- [20] Qianli Ma, Haotian Nan, Yeyun Gong, Can Luo, Chen Li, Chen Liang, Nan Duan, and Weizhu Chen. Let’s Reward Step by Step: Step-Level Reward Model as the Navigators for Reasoning. In *NeurIPS*, volume 36, pages 23145–23158, 2023.
- [21] William Peebles and Saining Xie. Scalable Diffusion Models with Transformers. In *ICCV*, pages 4172–4182, 2023.
- [22] Reiner Pope, Sholto Douglas, Aakanksha Chowdhery, Jacob Devlin, James Bradbury, Jonathan Heek, Kefan Xiao, Shivani Agrawal, and Jeff Dean. Efficiently Scaling Transformer Inference. In *MLSys*, 2023.
- [23] Reid Pryzant, Dan Iter, Jerry Li, Yin Tat Lee, Chenguang Zhu, and Michael Zeng. Automatic Prompt Optimization with "Gradient Descent" and Beam Search. In *EMNLP*, pages 7957–7968, 2023.
- [24] Zipeng Qi, Lichen Bai, Haoyi Xiong, and Zeke Xie. Not All Noises Are Created Equally: Diffusion Noise Selection and Optimization. *CoRR*, abs/2407.14041, 2024.
- [25] Tim Salimans, Ian J. Goodfellow, Wojciech Zaremba, Vicki Cheung, Alec Radford, and Xi Chen. Improved Techniques for Training GANs. In *NeurIPS*, pages 2226–2234, 2016.
- [26] David W. Scott. *Multivariate Density Estimation: Theory, Practice, and Visualization*. Wiley, 1992.
- [27] Charlie Snell, Jaehoon Lee, Kelvin Xu, and Aviral Kumar. Scaling LLM Test-Time Compute Optimally can be More Effective than Scaling Model Parameters. *arXiv preprint arXiv:2408.03314*, 2024.
- [28] Jiaming Song, Chenlin Meng, and Stefano Ermon. Denoising Diffusion Implicit Models. In *CLR*, 2021.
- [29] Robert Endre Tarjan. Depth-First Search and Linear Graph Algorithms. *SIAM J. Comput.*, 1:146–160, 1972.
- [30] Darshan Thaker, Abhishek Goyal, and René Vidal. Frequency-Guided Posterior Sampling for Diffusion-Based Image Restoration. *arXiv preprint arXiv:2411.15295*, 2024.

- [31] Keyu Tian, Yi Jiang, Zehuan Yuan, Bingyue Peng, and Liwei Wang. Visual Autoregressive Modeling: Scalable Image Generation via Next-Scale Prediction. In *NeurIPS*, 2024.
- [32] Aäron van den Oord, Oriol Vinyals, and Koray Kavukcuoglu. Neural Discrete Representation Learning. In *NeurIPS*, pages 6306–6315, 2017.
- [33] Evan Z. Wang, Federico Cassano, Catherine Wu, Yunfeng Bai, William Song, Vaskar Nath, Ziwen Han, Sean M. Hendryx, Summer Yue, and Hugh Zhang. Planning in Natural Language Improves LLM Search for Code Generation. In *ICLR*, 2025.
- [34] Xuezhi Wang, Jason Wei, Dale Schuurmans, Quoc V Le, Ed H Chi, Sharan Narang, Aakanksha Chowdhery, and Denny Zhou. Self-Consistency Improves Chain of Thought Reasoning in Language Models. In *ICLR*, 2023.
- [35] Jason Wei, Xuezhi Wang, Dale Schuurmans, Maarten Bosma, Brian Ichter, Fei Xia, Ed H. Chi, Quoc V. Le, and Denny Zhou. Chain-of-Thought Prompting Elicits Reasoning in Large Language Models. In *NeurIPS*, 2022.
- [36] Yangzhen Wu, Zhiqing Sun, Shanda Li, Sean Welleck, and Yiming Yang. Inference Scaling Laws: An Empirical Analysis of Compute-Optimal Inference for LLM Problem-Solving. In *ICLR*, 2025.
- [37] Yuxi Xie, Kenji Kawaguchi, Yiran Zhao, James Xu Zhao, Min-Yen Kan, Junxian He, and Michael Qizhe Xie. Self-Evaluation Guided Beam Search for Reasoning. In *NeurIPS*, 2023.
- [38] Shunyu Yao, Dian Yu, Jeffrey Zhao, Izhak Shafran, Tom Griffiths, Yuan Cao, and Karthik Narasimhan. Tree of thoughts: Deliberate problem solving with large language models. In *NeurIPS*, 2023.
- [39] Zihan Yu, Liang He, Zhen Wu, Xinyu Dai, and Jiajun Chen. Towards Better Chain-of-Thought Prompting Strategies: A Survey. *arXiv preprint arXiv:2310.04959*, 2023.
- [40] Yue Zhao, Yuanjun Xiong, and Philipp Krähenbühl. Image and Video Tokenization with Binary Spherical Quantization. *arXiv preprint arXiv:2406.07548*, 2024.